Evaluation of TRMM Rain Estimates Using Ground Measurements over Central Florida

JIANXIN WANG AND DAVID B. WOLFF

Science System and Applications, Inc., Lanham, and NASA Goddard Space Flight Center, Greenbelt, Maryland

(Manuscript received 14 April 2011, in final form 29 December 2011)

ABSTRACT

This study evaluates space-based rain estimates from the Tropical Rainfall Measuring Mission (TRMM) satellite using ground-based measurements from the radar (GR) and tipping-bucket rain gauges (TG) over the TRMM Ground Validation (GV) site at Melbourne, Florida. The satellite rain products are derived from the TRMM Microwave Imager (TMI), precipitation radar (PR), and combined (COM) rain algorithms using observations from both instruments. The TRMM satellite and GV rain products are spatiotemporally matched and are intercompared at multiple time scales over the 12-yr period from 1998 to 2009. On monthly and yearly scales, the TG agree excellently with the GR because the GR rain rates are generated using the TG data as a constraint on a monthly basis. However, large disagreements exist between the GR and TG at shorter time scales because of their significantly different spatial and temporal sampling modes. The yearly biases relative to the GR for the PR and TMI are generally negative, with a few exceptions. The COM bias fluctuates from year to year over the 12-yr period. The PR, TMI, and COM are in good overall agreement with the GR in the lower range of rain rates, but the agreement is notably worse at higher rain rates. The diurnal cycle of rainfall is captured well by all products, but the peak satellite-derived rainfall (PR, TMI, and COM) lags the peak from the ground measurements (GR and TG) by ~1 h.

1. Introduction

Accurate rain estimation at different spatial and temporal scales is important to meteorologists and hydrologists as well as to a wide variety of decision makers such as emergency managers, agriculturalists, and industrialists. This effort remains a major challenge for scientists working on rain-rate retrieval algorithms, however, because of the extreme spatial and temporal variability of precipitation and the costs of deploying the instrument infrastructure necessary to adequately sample precipitation over large areas. Since the launch of the Tropical Rainfall Measuring Mission (TRMM) satellite in November of 1997, a number of rainfall products have been produced from the active TRMM precipitation radar (PR) and passive Microwave Imager (TMI) sensors. To be sure, the PR, TMI, or any other sensor has both strengths and weaknesses. Rain products derived from the PR and TMI suffer substantial sampling, retrieval, and systematic errors. To improve TRMM rainfall algorithms and to help data users to be aware of the limitation of the TRMM products, it is necessary to validate TRMM products against other types of rainfall observations, such as more conventional ground-based radar (GR) and tipping-bucket rain gauge (TG) measurements.

The major difficulty with validating TRMM products using ground measurements is that the satellite and ground sensors measure fundamentally different quantities at different temporal–spatial resolutions. The TRMM satellite samples rainfall only approximately 1–3 times per day over a given location along its orbit, dependent on latitude and sensor. On the other hand, GR-based products provide areal coverage of precipitation over approximately 71 000 km^2 and a span of 5–10 min while TGs provide nearly continuous observations but only at a fixed location or ''point source.''

The TRMM PR is an electronically scanning Ku-band radar that measures the backscattered echo from precipitation and cloud particles. The PR rain retrievals are based on application of reflectivity–rain-rate (Z_e–R) relationships after correcting the PR reflectivity measurements for attenuation, selecting the default drop

Corresponding author address: Jianxin Wang, NASA/GSFC, Code 612, Greenbelt, MD 20771.
E-mail: jianxin.wang@nasa.gov

DOI: 10.1175/JAMC-D-11-080.1

size distribution model, and correcting for the nonuniform beam-filling effect (Iguchi et al. 2000). The PR has a horizontal resolution of nearly 5 km at the ground, vertical resolution of 0.25 km, and a swath width of 247 km. The TMI is a conically scanning microwave radiometer that measures the microwave radiation emitted by the earth's surface and by cloud and rain drops at five separate frequencies: 10.7, 19.4, 21.3, 37.0, 85.5 GHz. The TMI rain rates are retrieved using the Goddard profiling algorithm on the basis of a Bayesian technique that matches TMI brightness temperatures with hydrometeor profiles (Kummerow et al. 1996, 2001; Olson et al. 2006). The horizontal resolution of the TMI sensor varies from ~5 km for the highest frequencies to ~45 km for the lowest-frequency channels. The TMI has an 878-km-wide swath on the surface. Note that the abovementioned swath widths and horizontal resolutions are for the PR and TMI after August of 2001, when the TRMM orbit was boosted from 350 to 402 km to preserve fuel for extended life of the satellite. The resolutions for the PR and TMI were slightly better before the TRMM boost.

The GR transmits microwaves and then measures how much of the microwave energy is reflected back to the radar by objects in the air such as raindrops, snow crystals, hailstones, or even insects and dust. The area-averaged surface rainfall is subsequently estimated by converting quality-controlled reflectivity using Z_e–R relationships (Wolff et al. 2005). The GR used in this study is a Weather Surveillance Radar-1988 Doppler (WSR-88D) in Melbourne, Florida (KMLB). The KMLB radar has a varying range resolution of 0.25–1.0 km and a beamwidth of 0.5°–1° depending on the radar scan strategy.

The PR, TMI, and GR do not directly measure surface rainfall amounts, but rather they measure volume-integrated rain rates aloft over the area roughly equivalent to the instrument resolution, from which the rain rate is inferred. The TG, in contrast, is a simple mechanical device deployed on the surface to directly measure rainwater entering the gauge orifice in discrete quantities. A typical TG has a collection orifice of 0.254-m (10 in.) diameter and a bucket size corresponding to 0.254 mm (0.01 in.) of rainfall. This kind of TG subsequently gives surface rainfall amounts in a near-point area of 0.051 m^2 with a sampling resolution of 0.254 mm. Thus the TG makes what are essentially point measurements in space, with relatively high temporal resolution that varies from several seconds to a few minutes or even longer and that depends on the rain intensity and gauge bucket size. Intense rain quickly fills up the bucket, which results in higher temporal resolution. The TG has good temporal sampling, but its poor spatial sampling can lead to significant errors in estimates of area-averaged rain rates (e.g., Wang and Wolff 2010). On the other hand, the satellite has good spatial coverage but poor temporal sampling. The GR provides the best combination of temporal resolution and spatial coverage, but the GR rain estimation is based on a Z_e–R relationship that is usually established using direct measurements from gauges or disdrometers. The GR, as well as the TRMM PR and TMI, makes area-averaged observations, which may average localized intense-rain regions with nearby less-intense-rain regions or dry regions (i.e., incomplete or nonhomogeneous beam filling can average out the occurrences of the heavier precipitation features in highly variable precipitating systems).

Acknowledgment of the pros and cons inherent in each sensor has led to numerous efforts to combine them to take advantage of the strength of each sensor to produce the best possible precipitation products, including the Climate Prediction Center (CPC) Merged Analysis of Precipitation (CMAP; Xie and Arkin 1997), TRMM Multisatellite Precipitation Analysis (TMPA; Huffman et al. 2007), CPC morphing algorithm (CMORPH; Joyce et al. 2004), the Precipitation Estimation from Remotely Sensed Information Using Artificial Neural Network (PERSIANN; Hsu et al. 1999; Sorooshian et al. 2000), the Naval Research Laboratory Blended-Satellite Precipitation technique (NRLB; Turk and Miller 2005), the Global Satellite Mapping of Precipitation (GSMaP; Okamoto et al. 2007), Global Precipitation Climatology Project monthly precipitation (GPCP; Huffman et al. 1997; Adler et al. 2003), and National Severe Storms Laboratory's Next-Generation Quantitative Precipitation Estimation high-resolution national mosaic product (Q2; Vasiloff et al. 2007). The accuracy of the combined product heavily depends on quantitative understanding of the relative performance of different sensors. Many efforts have been made to intercompare and cross validate various satellite and ground rain products. For example, the TG measurements were applied to evaluate the GR rain product (e.g., Ciach and Krajewski 1999; Wang and Wolff 2010), the PR was utilized to calibrate GR (e.g., Anagnostou et al. 2001; Gabella et al. 2006; Wang and Wolff 2009), PR and TMI precipitation retrievals were compared with rain gauge data on ocean buoys (Serra and McPhaden 2003; Bowman 2005) and land surfaces (Fisher 2004, 2007), and a number of merged satellite rain products were evaluated against ground measurements (e.g., Ebert et al. 2007; Tian et al. 2007; Wolff and Fisher 2008; Dinku et al. 2010; Sohn et al. 2010). Some of these studies were based on comparisons over central Florida. Amitai et al. (2005) evaluated probability distribution functions (PDF) of rain rates from the TRMM PR using collocated data from GR over central

Florida. The evaluation showed that the PR underestimated 4% of rain amount and missed 4.5% of rain occurrence, as compared with the GR. Fisher (2007) showed that in central Florida the TMI rain estimate was highly correlated with and reasonably agreed with the TG- and GR-derived rain parameters, whereas the PR estimate appeared to be more variable. Wolff and Fisher (2008) compared TRMM rain rates with ground data over Melbourne, Florida (as well as Kwajalein Atoll) and revealed that the PR, TMI, and COM agreed well with GR at the lower rain rates but that there were some notable differences at the higher rain rates. Comparing the different types of measurement schemes for satellite-based and ground-based sensors can be challenging because too much uncertainty is involved in the comparison because of their distinctly different sampling characteristics. The highly successful TRMM ground validation (GV) program has provided nearly 14 years of continuous rainfall observations, which makes it possible to provide quantitative comparisons among the spaceborne observations and ground-based measurements with greater certainty and statistical robustness.

The objective of this study is to advance our understanding of the relative differences in various data sources. We use 12 years (1998–2009) of GR product 2A53 and TG product 2A56 for comparison with coincident TRMM product 3G68 over the GV site at Melbourne, Florida (MELB). The descriptions of TRMM products are available online (http://pmm.nasa.gov/data-access/data-products). The data are matched at 0.25° × 0.25° grid resolution and various time scales. Section 2 describes the TRMM and GV data used in this study. Section 3 gives results of evaluations and comparisons among the TRMM satellite, GR, and TG products at multiple time scales. The ability of each product to represent the diurnal cycle is also assessed. A summary and conclusions are provided in section 4.

2. Data

a. GV data

Figure 1 is a geographical map of the radar and rain gauge networks at MELB. The KMLB radar is located at 28.1133°N, 80.6542°W and is plotted as a large dot at the center of the map. Also plotted are 0.25° × 0.25° grids and radar range rings at 50, 100, and 150 km. There are three TG networks at MELB: Kennedy Space Center (KSC), South Florida Water Management District (SFL), and St. John's River Water Management District (STJ). The KSC gauges (small dots) are owned and operated by the National Aeronautics and Space Administration (NASA). Both the SFL (squares) and STJ (triangles) gauges are operated by their respective Florida water management districts. The number of active gauges changed from time to time over the period of this study; quite a few new gauges were installed in the networks, and several gauges were removed or were inoperable. As of this writing, there are 31, 84, and 34 active gauges regularly reporting rain tips at KSC, SFL, and STJ, respectively, within 150 km of the KMLB radar. The distances between the KMLB radar and all KSC gauges range from 30 to 70 km, whereas 128 SFL and 37 STJ gauges are beyond the 150-km range. This study only uses the 149 gauges within 150 km of the radar. The overall gauge density is very good, but these gauges are unevenly distributed across the study area, and no gauges exist 100 km west of the radar or over the Atlantic Ocean. There are 49 of the 0.25° grids that have at least one gauge. The number of gauges in each of these 49 grids varies from 1 to 23, with an average of 3. All gauges are tipping-bucket gauges with a resolution of 0.254 mm per tip. The KSC and STJ gauges report rain tips at a sampling resolution of 1 s, whereas some SFL gauges sample rainfall at the resolution of 1 min and others at 5 min.

There are difficult challenges in accurately measuring rainfall with gauges because of limited spatial sampling; systematic, mechanical, and electrical problems; calibration issues; and so on (e.g., Sieck et al. 2007; Wang et al. 2008; Wang and Wolff 2010). In this study, unreliable gauge tip records are detected and removed through careful quality control of the raw gauge data, and then the 1-min rain rates (2A56), provided in the TRMM Science Data Product, are derived from the quality-controlled tip records by using a cubic spline–based algorithm (Wang et al. 2008). Further quality control is conducted by comparing 2A56 rain rates with radar-reflectivity data over the gauge locations to remove ''bad gauges'' on a monthly basis (Amitai 2000). This procedure removes 31.6% of monthly 2A56 files over the period. Only the reliable 2A56 rain rates from ''good gauges'' that passed these two quality-control steps are used in this study to compare with radar and satellite rain products.

The GV radar-rain product used is the TRMM 2A53 at the MELB GV site. The 2A53 consists of instantaneous rain rates with a 2 km × 2 km horizontal resolution and covers a circular region with a radius of 150 km from the KMLB radar. The radar rain rates are generated using Z_e–R relations derived from the window probability matching method (WPMM; Rosenfeld et al. 1994). The WPMM employs quality-controlled radar reflectivities and gauge rain rates and forces the matching of their respective monthly PDFs. Because the KMLB radar takes about 5 min to complete a volume scan, the 2A53

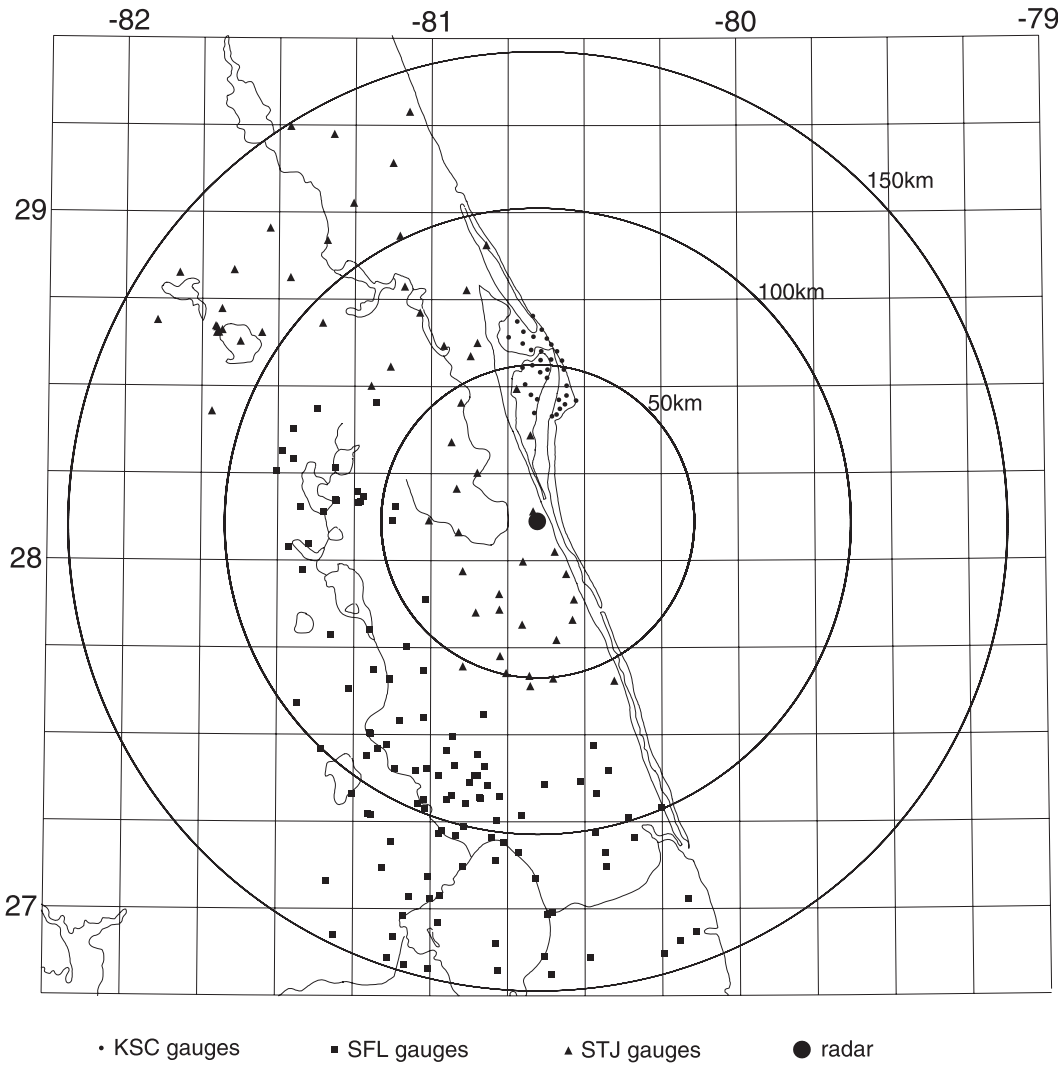

FIG. 1. Map of the KMLB radar and three rain gauge networks (KSC, SFL, and STJ) for the GV site at Melbourne. The KMLB radar at the center of the map is plotted as a large dot. The KSC, SFL, and STJ gauges are plotted as small dots, squares, and triangles, respectively. Also plotted are 0.25° grids and radar range rings at 50, 100, and 150 km.

instantaneous rain-rate maps are available approximately every 5 min. Rain accumulations at time scales of 5 min or larger can be obtained by integrating the 2A53 maps over the time difference between consecutive radar scans. If the time difference exceeds 12 min, the 2A53 maps are integrated forward for 5 min.

The KMLB radar is well maintained and is relatively stable (Wang and Wolff 2009), yet it experienced numerous downtimes during this 12-yr period of study, possibly because of hardware and software problems, electrical failures, and planned maintenance. The radar downtimes introduce data gaps in the series of volume scans that negatively bias the radar rain integration. Because consecutive scans very often occur 11–12 min apart when the KMLB radar operates in clear-air mode, we define a gap as the time difference between any two consecutive scans that are separated by 13 min or longer. Table 1 gives yearly KMLB radar gap statistics and missing-rain percentages resulting from the gaps in the period from 1998 to 2009. The missing-rain percentages are estimated from the percentages of gauge rainfall during the radar gaps. The yearly total radar gap length roughly decreases from 971.4 h in 1998 to 190.6 h in 2009. There are a total of 9250 gaps composing a total length of 6999.8 h during the period, which accounts for 6.65% of the period. The individual gap length ranges from 0.2 to 173.8 h, with a mean of 0.8 h. The gaps falling in rainy periods result in about 6.46% missing rain in the 12-yr rainfall accumulation. In summary, the radar data gap is not a serious problem with regard to the overall bias of

TABLE 1. Yearly KMLB radar gap statistics and missing-rain percentages due to the gaps. The missing-rain percentages are estimated from the percentage of gauge rainfall during the radar gaps.

Year	No. of gaps	Total gap length (h)	Mean gap length (h)	Largest gap (h)	Gap %	Missing rain (%)
1998	913	971.4	1.1	70.6	11.09	17.71
1999	1133	578.6	0.5	24.5	6.60	8.13
2000	1255	670.6	0.5	83.5	7.63	13.36
2001	1134	760.5	0.7	173.8	8.68	10.77
2002	1192	831.7	0.7	58.5	9.49	4.63
2003	718	716.8	1.0	144.2	8.18	4.21
2004	721	756.2	1.0	99.9	8.61	11.42
2005	642	338.3	0.5	19.0	3.86	2.77
2006	697	512.3	0.7	78.2	5.85	2.31
2007	255	284.6	1.1	30.9	3.25	2.34
2008	416	388.2	0.9	32.4	4.42	3.53
2009	174	190.6	1.1	18.4	2.18	3.06
Tot	9250	6999.8	0.8	173.8	6.65	6.46

radar-rain estimation. Nevertheless, all radar gaps are excluded in comparisons among the radar, gauge, and satellite rainfall.

b. TRMM data

The TRMM 3G68 version-6 product consists of three principal surface rain-rate estimates derived from the PR only, TMI only, and PR–TMI combined (COM) algorithms. The data are nearly instantaneous rain rates that are spatially averaged within each 0.25° × 0.25° grid where a TRMM overpass occurs (Stocker et al. 2001). Operating at 13.8 GHz, the TRMM PR suffers significant attenuation at lower levels, especially in convective rain (e.g., Wang and Wolff 2009). The attenuation is corrected using a hybrid method of the Hitschfeld–Bordan iterative scheme (Hitschfeld and Bordan 1954) and a surface reference technique (Iguchi and Meneghini 1994). Details of the PR algorithm are available in Iguchi et al. (2000). The PR provides information on the three-dimensional structure of rain systems with its high horizontal (~5 km at nadir after TRMM boost) and vertical (0.25 km) resolutions. The swath width of the PR, however, is only around one-third of the TMI swath width, which results in limited sampling for many climate applications.

The TMI rain rates are estimated using the Goddard profiling algorithm (Kummerow et al. 1996, 2001; Olson et al. 2006). The COM algorithm combines the rain information from both PR and TMI to take advantage of the relative strength of each sensor and, it is hoped, to result in a more accurate product than either the TMI or PR rain product by itself (Haddad et al. 1997; Smith et al. 1997). TRMM only provides a series of snapshots of rainfall along its orbit track, and those snapshots are taken only about 1–3 times per day over a given location depending on its latitude and sensor. Thus, the PR and TMI only provide limited rain samples over a given location. Therefore, the sampling error of the satellite-inferred rainfall is a significant issue.

c. Spatiotemporally matching TRMM and GV data

The TRMM 3G68 has a spatial resolution of 0.25° × 0.25°; thus the GR and TG products must be also averaged to the same spatial resolution for fair comparisons with the 3G68. There are 49 of the 0.25° grids that have at least one gauge over the circular area with radius of 150 km centered on the GR (Fig. 1). Because the GR 2A53 rain maps are available about every 5 min and are calibrated against the TG data on a monthly basis, we integrate GR rain rates to various time scales ranging from 5 min to 30 days. To correspond, the TG, PR, TMI, and COM rain rates are also individually integrated over these time scales whenever the data are available, regardless of the TRMM overpass time.

Comparisons can be carried out by properly averaging each product in space and time (Bowman 2005). The TRMM 3G68 data are generated by spatially averaging within each 0.25° × 0.25° grid and temporally averaging within a very short time period for the TRMM sensors to scan through the grid. In addition, there is an implicit averaging time due to the fact that the TRMM rain rates at the earth's surface are derived from volume-integrated measurements of hydrometeors at altitudes above the surface. This averaging time is related to the time required for raindrops to fall to the earth's surface. Furthermore, rainfall observations are correlated in time and space domains. Therefore, comparisons among different rain products can be improved by properly averaging in space and time. As discussed earlier, the TRMM samples rainfall only at discrete time intervals. Limited temporal sampling can result in significant errors in estimates of time-integrated rain rates. It is necessary to

TABLE 2. Mean yearly area rain rates (mm h^{-1}) from the GR, TG, PR, TMI, and COM, and biases (%) for TG, PR, TMI, and COM relative to the GR over the 12-yr period from 1998 to 2009.

Year	GR	TG	PR	TMI	COM	TG bias	PR bias	TMI bias	COM bias
1998	0.1449	0.1410	0.1087	0.1489	0.1562	−2.66	−24.98	2.79	7.80
1999	0.1622	0.1627	0.1659	0.1481	0.2066	0.27	2.25	−8.74	27.33
2000	0.0986	0.1029	0.0739	0.0701	0.0914	4.38	−25.04	−28.89	−7.27
2001	0.1588	0.1575	0.1137	0.1345	0.1463	−0.81	−28.38	−15.26	−7.85
2002	0.2160	0.2239	0.1466	0.1416	0.1932	3.65	−32.13	−34.43	−10.57
2003	0.1478	0.1512	0.1456	0.1726	0.1901	2.32	−1.50	16.75	28.61
2004	0.1456	0.1439	0.1218	0.1803	0.1537	−1.20	−16.35	23.80	5.56
2005	0.1720	0.1697	0.1003	0.1091	0.1310	−1.30	−41.66	−36.55	−23.81
2006	0.1133	0.1118	0.0974	0.0914	0.1254	−1.27	−14.00	−19.31	10.75
2007	0.1356	0.1346	0.0814	0.1068	0.1085	−0.78	−40.01	−21.29	−20.04
2008	0.1539	0.1519	0.1390	0.1543	0.1833	−1.29	−9.66	0.24	19.09
2009	0.1405	0.1421	0.0742	0.1109	0.1043	1.15	−47.16	−21.04	−25.77
1998–2009	0.1478	0.1478	0.1142	0.1311	0.1493	0.04	−22.74	−11.30	1.04

study the dependence of correlation, bias, and sampling issues on the time averaging applied to the satellite and GV data. For this purpose, the TRMM satellite data are matched with GV data at 0.25° spatial resolution and from 5-min to 30-day temporal scales. Statistics are presented in sections 3a–e for comparing GV rain measurements (GR and TG) with the TRMM satellite rain estimates (PR, TMI, and COM) at various time scales.

3. Evaluation and intercomparison

In this section, the TRMM PR, TMI, and COM rain rates are intercompared with the GR and TG data at 0.25° grid resolution and various time scales over MELB. The MELB site is located in the subtropics on the Atlantic coast of central Florida. As one of the four major sites for TRMM GV operation, the ground validation at MELB plays an important rule in evaluating the performance of the TRMM rain retrieval algorithms (Wolff et al. 2005).

a. Mean yearly rain rates

Table 2 lists mean yearly area rain rates at MELB from each product (GR, TG, PR, TMI, and COM) over the period (1998–2009). The biases, in percentage, for the TG, PR, TMI, and COM relative to the GR are also listed. Using the GR rain rate as an empirical reference, the bias is defined as

$$\text{bias} = \frac{E - R}{R} \times 100\%, \tag{1}$$

where R is the mean GR rain rate and E is the mean rain rate from the TG, PR, TMI, or COM. The mean rain rate is individually calculated for each product by equally averaging all available samples. Only grids containing gauges that passed the quality control are used in the calculation of Eq. (1). Data during the GR gap periods are not included in the computation.

Because the GR rain rates are estimated using monthly Z_e–R relationships, mean rain rates of the GR and TG shown in Table 2 exhibit excellent agreement for each year, with a 12-yr average bias of 0.04%. The yearly bias for the PR is predominantly negative. The TMI bias is more variable, with negative values in 8 of 12 years. The 12-yr average biases are −22.74% and −11.30% for the PR and TMI, respectively. The COM bias fluctuates from year to year but most closely matches the GV (TG and GR) mean rain rates, with an average bias of only 1.04%.

b. Average monthly rain rate

The MELB site receives most of its yearly rainfall between June and September from sea-breeze-induced isolated convective systems and tropical systems (easterly waves as well as tropical cyclones). The yearly rainfall budget is also contributed to by mid-latitude frontal systems during winter months (Wolff et al. 2005). Figure 2 shows the average monthly rain rates at MELB estimated from the GR, TG, PR, TMI, and COM over the period from 1998 to 2009. As expected, the two GV products (GR and TG) appear to be nearly identical. As seen in Fig. 2, about 57% of the annual rainfall observed by the GR, TG, PR, or COM occurs in June–September. The TMI overestimates this percentage by about 68% but underestimates rain rates in all other months. The TMI algorithm does not work well over coastal land surfaces because of uncertainties in the surface emissivity. Relative to the GR and TG, the PR rain rates are lower in 11 out of 12 months. The negative PR bias is attributed to underestimation of higher rain rates by the PR algorithm, as will be shown in Table 3. In general, GV and

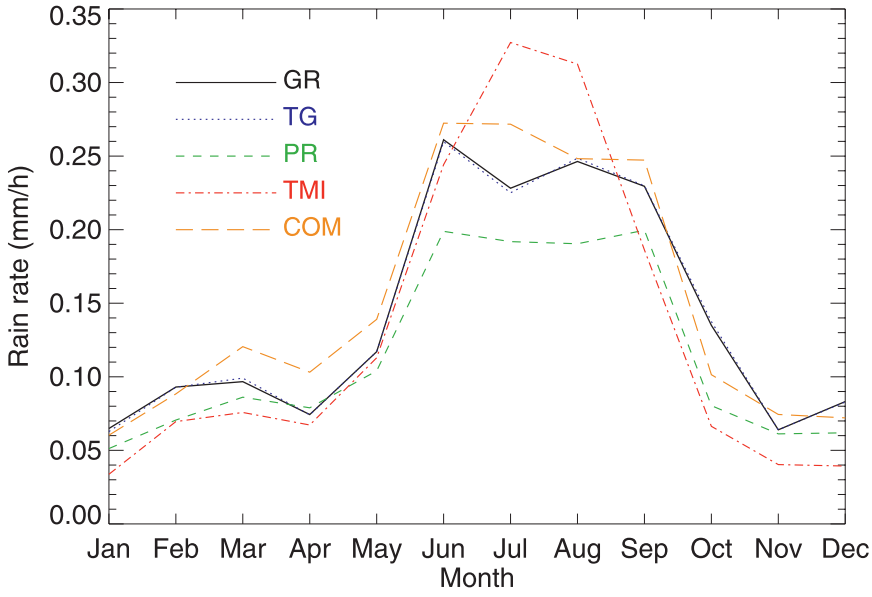

FIG. 2. Monthly average rain rates at MELB estimated from the GR, TG, PR, TMI, and COM over the period from 1998 to 2009.

satellite rain rates exhibit reasonably good agreement, with some notable exceptions, during the rainy season.

c. *Diurnal variations*

The rainfall diurnal variation is a pronounced component of the atmosphere over most regions of the earth, particularly over land, and is manifested in many meteorological variables. A comprehensive understanding remains uncertain, however, and is not well represented by numerical simulations (e.g., Betts and Jakob 2002; Nesbitt and Zipser 2003; Yang and Smith 2006) because of the limited observations and complex interactions between dynamic and radiative forcings. The availability of 12 years of TRMM satellite and GV rainfall products has provided an opportunity to analyze rainfall diurnal variability with greater certainty.

The precessing non-sun-synchronous orbit of TRMM allows it to sample the entire diurnal cycle in a period of about 46 days (47 after TRMM boost). TRMM overpasses over a given location with significant precipitation occurring are relatively infrequent, however, and thus spatial–temporal averaging of rain rates with sufficient samplings over a long time period must be performed to reconstruct representative diurnal features over a small geographic scale. Figure 3 shows the annual diurnal cycle of rain rates from the satellite (TRMM PR, TMI, and COM) and ground measurements (GR and TG) averaged over all 0.25° grids at MELB over the period of study. The averaged rain rates are calculated at 1-h intervals and are plotted at the endpoint of each local hour [eastern standard time (EST)] in Fig. 3. A 3-h running average is applied in this figure to reduce noise. Largely because of the TRMM discrete temporal sampling in this small area, the PR, TMI, and COM display small variations at time scales of a few hours.

The GR 2A53 algorithm is designed in such a way that the monthly PDF of the GR rain rates is matched to the PDF of the TG rain rates (Rosenfeld et al. 1994). Although no time adjustment is made to the GR data, the

TABLE 3. Number of matched pairs of the GR and other (TG, PR, TMI, or COM) rain rates at 5-min time scale and 0.25° grid resolution over the 12-yr period from 1998 to 2009. Also listed are biases for TG, PR, TMI, and COM relative to the GR and correlation coefficients (Corr) between the GR and other (TG, PR, TMI, or COM) rain rates.

	Lower rain rates ($\leq$10 mm h^{-1})			Higher rain rates ($>$10 mm h^{-1})			All rain rates ($\geq$0 mm h^{-1})		
	No. of matches	Bias (%)	Corr	No. of matches	Bias (%)	Corr	No. of matches	Bias (%)	Corr
TG	36 587 923	4.29	0.43	98 811	−10.46	0.26	36 686 734	0.04	0.52
PR	117 643	2.58	0.83	284	−46.50	0.50	117 927	−11.88	0.84
TMI	393 072	8.83	0.63	989	−34.01	0.39	394 061	−3.82	0.71
COM	117 643	29.33	0.80	284	−17.54	0.59	117 927	15.53	0.84

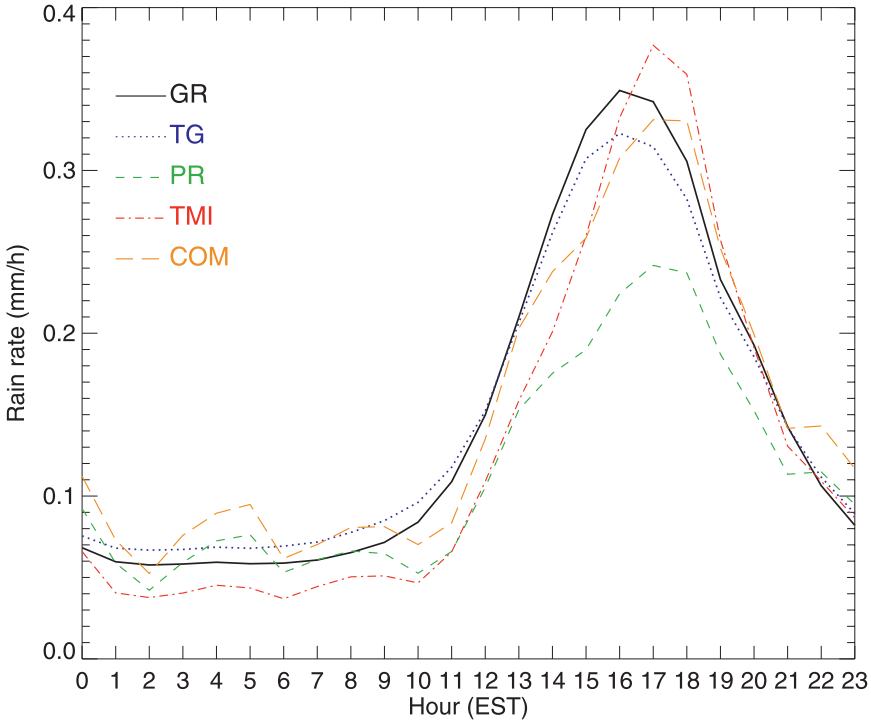

FIG. 3. The annual diurnal cycle of rain rate from the satellite (TRMM PR, TMI, and COM) and ground measurements (GR and TG) at MELB in the 12-yr period of 1998–2009. The rain rates are averaged over all 0.25° grids at 1-h intervals and are plotted at the endpoint of each local hour (EST). A 3-h running average is applied to reduce noise.

GR and TG are in very good agreement in phase as well as in amplitude (Fig. 3). Figure 3 also shows that both satellite and GV rain rates clearly depict a strong diurnal cycle. A distinct maximum occurs in the mid- to late afternoon (1500–1800 EST), which is largely a result of sea-breeze-induced convection. A nocturnal (0000–0300 EST) minimum in the cycle occurs when the boundary layer is most stable. The MELB site receives 57.4%, 53.7%, 51.1%, 63.0%, and 53.2% of its daily rainfall between 1400 and 2000 EST, as derived from the GR, TG, PR, TMI, and COM, respectively. Relative to GV, the TMI diurnal peak is overestimated while the PR peak is underestimated. The GR and TG data show a maximum at 1600 EST, whereas all TRMM satellite estimates display the maximum at 1700 EST. The satellite estimates lag the GV measurements by 1 h, which is overall consistent with other studies (Negri et al. 2002; Sohn et al. 2010). Negri et al. (2002) investigated the diurnal variation of TRMM rain estimates and the relative contributions from the convective and stratiform components over northern South America. Their result shows that the 1-h lag is mainly due to an inaccurate identification of the convection onset.

Figure 4 presents the diurnal features of rain rates on a seasonal basis. Spring (March–May), summer (June–August), and autumn (September–November) display a distinct diurnal cycle with a maximum in mid- to late afternoon and a minimum from midnight to early morning. Similar to the annual analysis, there is a 1-h lag between the satellite and GV rain rates in each of these three seasons. Summer has the most pronounced diurnal cycle, followed by autumn and spring. The annual diurnal cycle, as well as the annual rain budget, is largely dominated by summer rainfall. Neither satellite nor ground rain products reveal a strong diurnal cycle in winter (December–February) rain rates (upper-left panel of Fig. 4) because the daytime land heating and its induced sea/land breeze are weak at MELB during wintertime.

d. Mean rain-rate profiles from 5-min to 30-day scale

Scatterplots are often employed to compare all pairs of concurrent rain measurements from two sensors. They can be noisy, however, because the large number of data pairs can crowd the plot. An alternative graph, such as the mean rain-rate profile for each product (TG, PR, TMI, or COM), is constructed for comparison with the GR. Here the GR rain rates are used as an empirical reference. The profile is generated by first grouping rain rates matched at each 0.25° grid for the

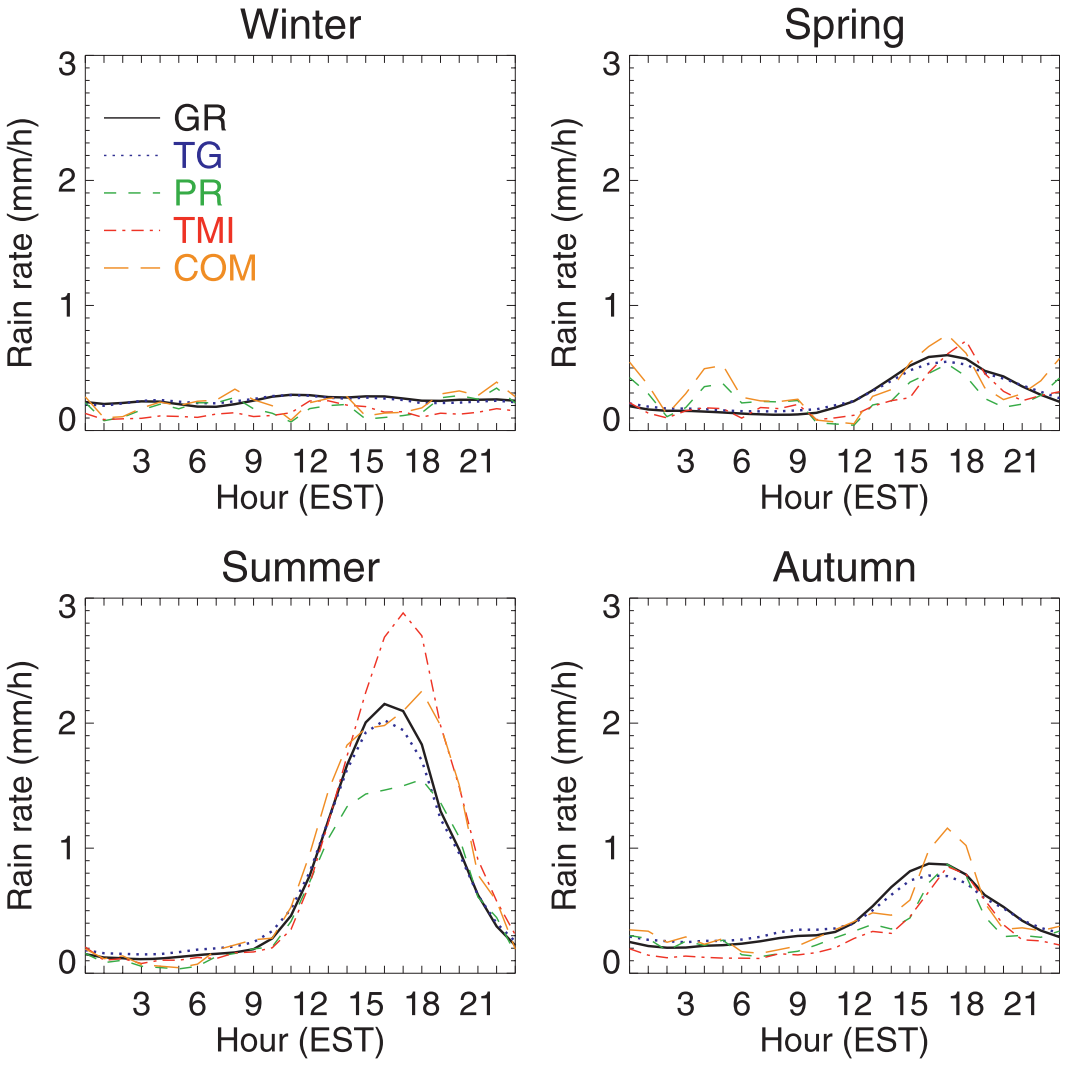

FIG. 4. As in Fig. 3, but for each season.

GR and each of other four products at a given interval, with respect to the GR rain rate. The interval is set to 1 mm h^{-1} at time scales ranging from 5 min to 12 h, to 0.5 mm h^{-1} from 1 to 2 days, and to 0.25 mm h^{-1} from 5 to 30 days. The matched rain rates in each group are then linearly averaged for each GR rain-rate interval. All pairs of the group-averaged rain rates for the GR and each of the other products (TG, PR, TMI, and COM) are plotted to form a mean rain-rate profile. Figure 5 shows mean rain-rate profile comparisons for the TG, PR, TMI, and COM at various time scales ranging from 5 min to 30 days. As expected, the TG compares very well to the GR. The TG bias relative to the GR fluctuates in a very narrow range between −0.55% and 0.16%. The TRMM PR and TMI rain estimates are generally lower than GV rain rates, whereas the COM estimates are higher than GV rain rates. The overall feature of Fig. 5 is consistent with the mean rain-rate profiles of Wolff and Fisher (2008) and scatterplots of Bowman (2005). The result could be different from other studies, however, because the rainfall error statistics can be highly regime dependent (e.g., Nesbitt et al. 2004; Berg et al. 2006).

In general, Fig. 5 illustrates that the PR, TMI, and COM are in good overall agreement with respect to the GR in the lower range of rain rates. The linear correlation between the GR and each of the other products drops with increasing rain intensity. The agreement is much poorer in the higher range of rain rates. Table 3 quantitatively shows the relative biases of each product (TG, PR, TMI, or COM) with respect to the GR at lower ($\leq$10 mm h^{-1}), higher (>10 mm h^{-1}), and all ($\geq$0 mm h^{-1}) ranges of rain rates. The TG, PR, TMI, and COM overestimate the lower rain rates and underestimate

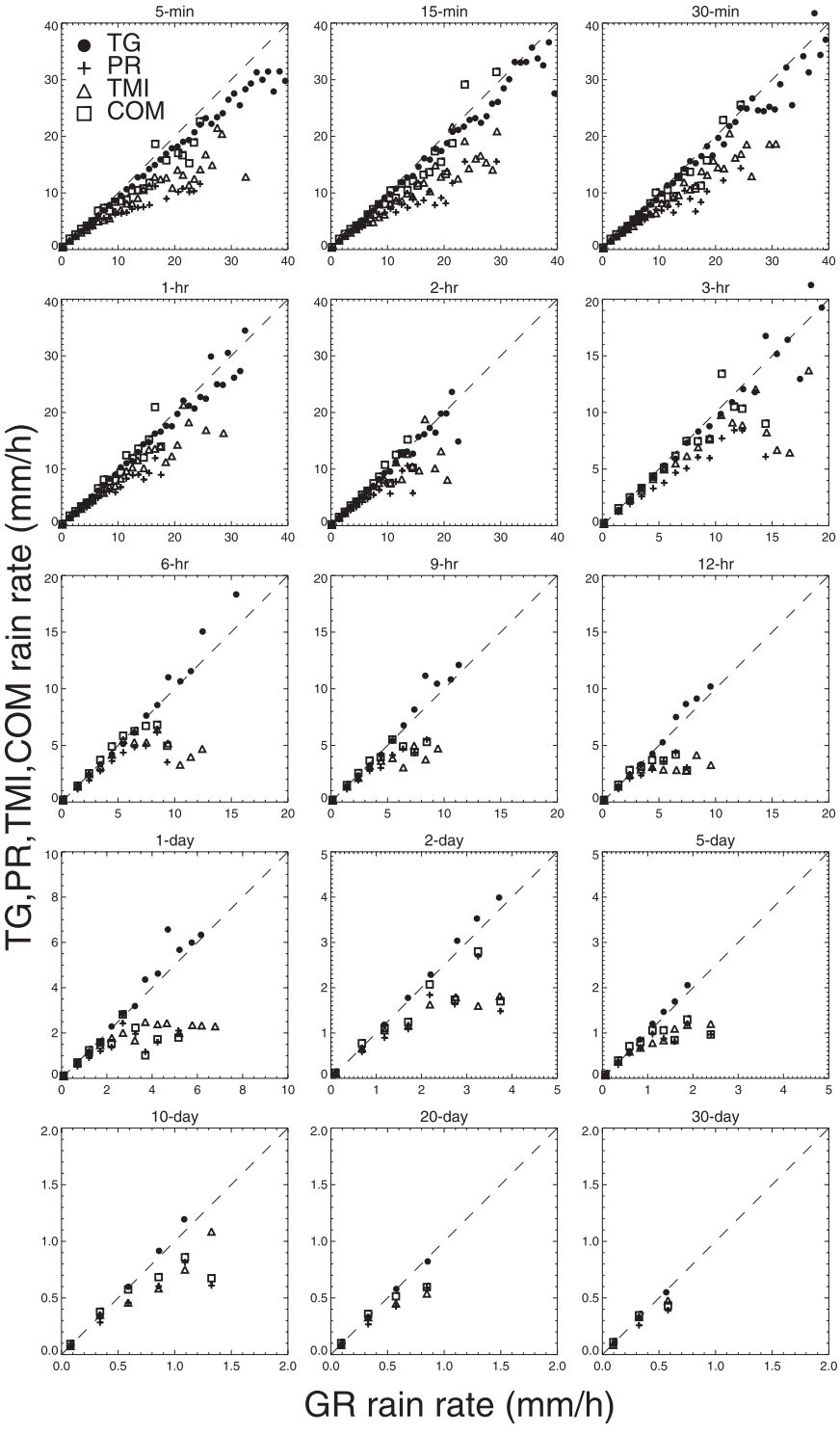

FIG. 5. Comparisons of the TG, PR, TMI, and COM mean rain rates with the GR mean rain rates at various time scales ranging from 5 min to 30 days. The diagonal line represents a one-to-one relationship.

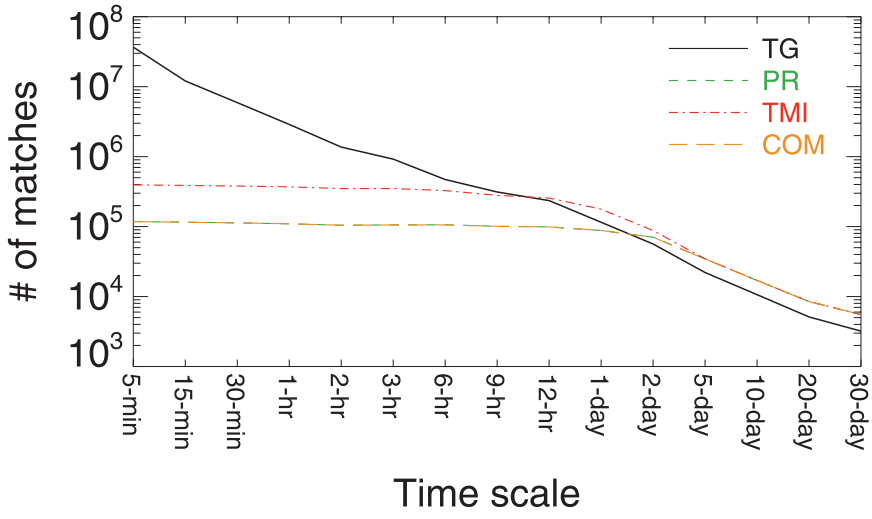

FIG. 6. Number of matched pairs of the GR and other (TG, PR, TMI, or COM) mean rain rates at the 0.25° grid resolution and various time scales over the 12-yr period from 1998 to 2009.

the higher rain rates. The substantial underestimation of the higher rain rates by the PR and TMI results in their respective overall negative biases. The underestimation of the PR and TMI at higher rain rates relative to the GR over land and coastal Florida was also reported by Wolff and Fisher (2008).

In the analysis of rain profiles, it is worth noting that the number of matched pairs of higher rain rates is only about 0.3% of the number of the matched lower rain rates at 5-min time scale and 0.25°grid resolution (Table 3). Rain rates of greater than 10 mm h^{-1} are less frequently observed at the 0.25° grid resolution for the PR and TMI. The sampling features for the TRMM satellite and GV sensors are essentially different. As displayed in Fig. 6, the number of matched pairs of the TG and GR rain rates at 0.25° grid resolution and 5-min time scale is as large as 3.7×10^7. The number is two orders of magnitude smaller for the matched pairs of the TMI and GR rain rates and is even smaller for the PR and GR pairs because of the narrower swath of the PR (~247 km) relative to the TMI (~878 km). The number of matched COM and GR pairs is the same as that of the PR and GR pairs because the COM algorithm is applied over the PR swath domain. As the time scale increases from 5 min to 30 days, the number of matched pairs of the GR and TG mean rain rates over each time scale steadily decreases. Because more instantaneous observations are included in the increasing time scale, the sampling errors decrease. As a result, the correlation between the GR and TG increases from 0.52 at 5-min scale to 0.93 at 30-day scale (top panel of Fig. 7). For the TRMM PR, TMI, and COM, however, the results are very different. Because the TRMM typically visits this study area (Fig. 1) about once per day, the TRMM overpasses included in calculating mean rain rates for each time scale from 5 min to 1 day are almost identical. Therefore, there is little change in the number of matches between the GR and TRMM samples (PR, TMI, or COM) as the time scale increases from 5 min to 1 day (Fig. 6). The correlations between the GR and TRMM (PR, TMI, and COM) rain rates decrease with increasing time scale (top panel of Fig. 7), however. This is due to the fact that as the time scale increases the GR increasingly includes samples that are further from the time of the TRMM overpasses and are thus not well correlated with the rain observed by the TRMM sensors. As the time scale further increases beyond 1–2 days, more TRMM overpasses are included in the analysis. The sample size of instantaneous observations consequently grows, and the sampling error decreases. Therefore, the correlations between the GR and TRMM (PR, TMI, and COM) rain rates improve. Note that the number of matches between the GR and other rain estimates (TG, PR, TMI, or COM) in Table 3 or Fig. 6 is fewer than the maximum possible. This is because the data (TG, PR, TMI, and COM) in the GR gap periods are not included in the analysis, and the data from ''bad gauges'' are excluded from matching the TG with GR.

To assess further the relative performance of different products, we also compute the relative error for the TG, PR, TMI, or COM rain rate with respect to GR rain rate at various time scales from 5 min to 30 days. Similar to Bowman (2005), the relative error ε in percentage is defined as

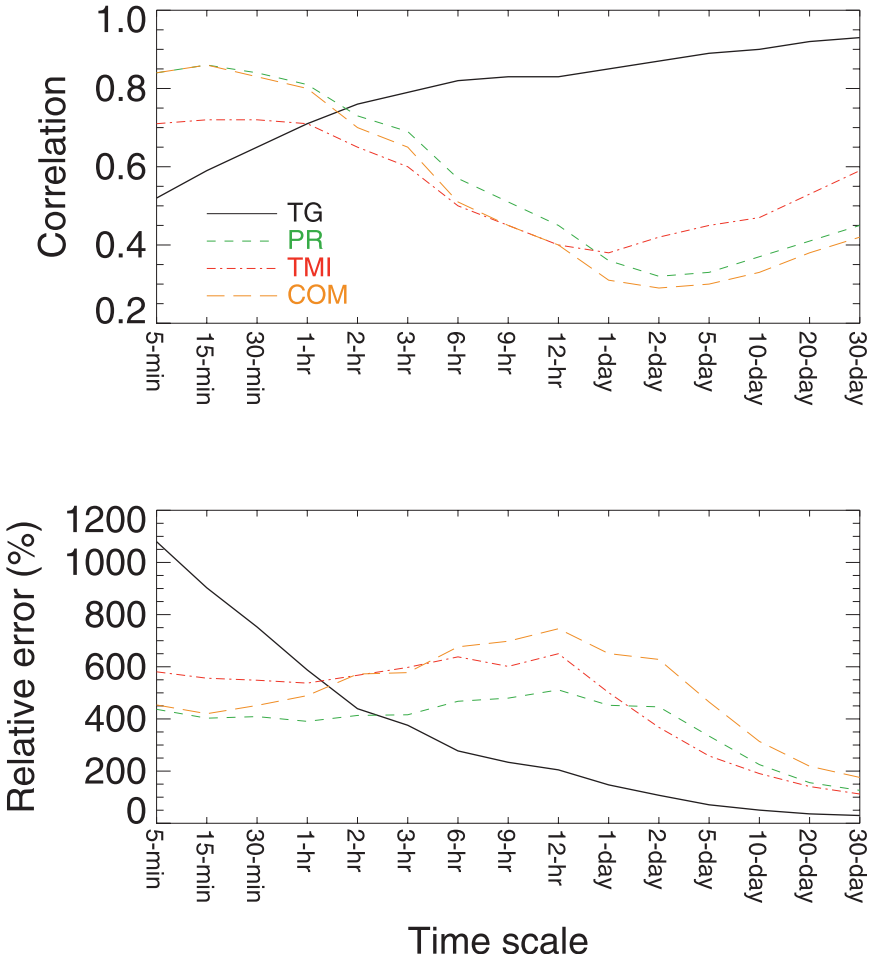

FIG. 7. (top) Correlation coefficient between the GR and other (TG, PR, TMI, or COM) mean rain rates at various time scales from 5 min to 30 days. (bottom) Relative error for TG, PR, TMI, or COM mean rain rates with respect to GR mean rain rates at various time scales from 5 min to 30 days.

$$\varepsilon = (\sigma/R) \times 100\%, \tag{2}$$

where R is the mean GR rain rate and σ is the root-mean-square difference between GR rain rate R_i and rain rate E_i from TG, PR, TMI, or COM. The σ can be calculated from n pairs of the GR and other (TG, PR, TMI, or COM) rain rates as follows:

$$\sigma = \sqrt{\frac{1}{n}\sum_{i=1}^{n}(E_i - R_i)^2}. \tag{3}$$

The relative error in Fig. 7 (bottom panel) is consistent with the correlation coefficients shown in the top panel. As the time scale increases from 5 min to 30 days, the relative error for TG monotonically decreases from 1079.6% to 29.7%. The relative error for the TRMM PR, TMI, or COM, however, increases to a maximum at 12-h to 1-day scale and then decreases to a minimum at 30-day scale. In comparison with Bowman 2005, the relative error for the TMI in Fig. 7 of this study is lower because GR mean rain rates are utilized as a reference in this study, whereas rain rates from each buoy-based gauge are used in Fig. 9 and Tables 1 and 2 of Bowman 2005.

e. *Skill scores*

Satellite validation is perhaps easier to understand with reference to rain categorical detection. Analysis of the detection skill scores is needed to provide a more complete scenario for algorithm rain estimates. A direct and intuitive skill score of categorical detection is the critical success index (CSI; Wilks 1995). The CSI is frequently used to compare rain detection abilities among different products, especially when rain occurrence is substantially less than

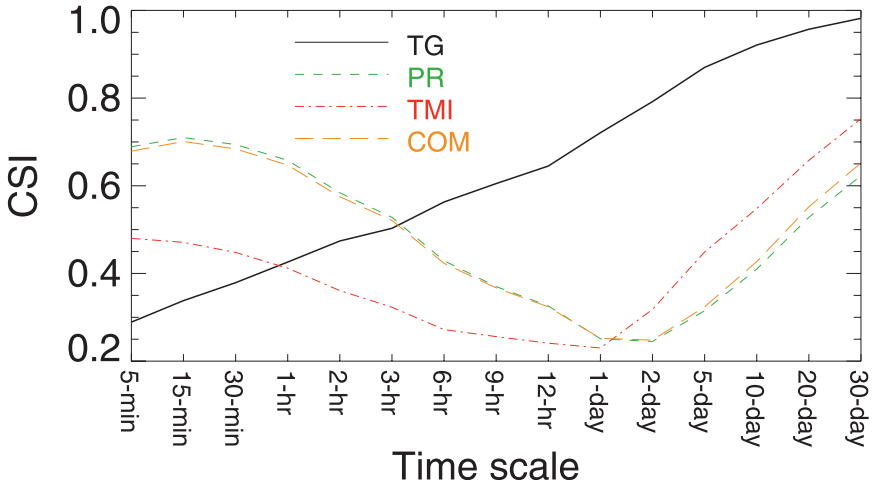

FIG. 8. The CSI as a function of time scale for the TG, PR, TMI, or COM. The rain-rate threshold of 0.01 mm h^{-1} is used to discriminate rain and no rain.

no-rain occurrence. To examine how well a rain product (TG, PR, TMI, or COM) detects rain, we use the GR as a reference and classify each 0.25° grid as a hit (the product correctly detects the GR observed rain), miss (the product fails to detect the GR observed rain), or false alarm (the product falsely detects rain that is not observed by the GR). The CSI is defined as

$$\mathrm{CSI} = \frac{H}{H + M + F}, \tag{4}$$

where H, M, and F are the numbers of hits, misses, and false alarms, respectively. A rain-rate threshold of 0.01 mm h^{-1} is used to discriminate rain and no rain for each product. In the perfect situation, $M = 0$ and $F = 0$ and thus CSI = 1. The worst possible CSI is 0. The CSI as a function of time scale for each product is plotted in Fig. 8. The PR exhibits an almost-identical CSI plot as the COM. The result for the TMI is similar to the PR and COM. The result for the TG is very different, however. The TG gives rain measurements only when rainwater in the bucket is filled, whereas the GR, PR, or TMI instantaneously observes rainfall during its scan. It is always the case that the TG will not record any rain activity in a short time period after rain starts until the bucket is full. The TG 2A56 algorithm tries to estimate the start time of a rain event through the cubic-spline interpolation, but the problem remains there although it is somewhat mitigated (Wang et al. 2008). In addition, the TG represents just one or a few discrete points within the grid, whereas the GR, PR, TMI, and COM rain rates are area averaged over the grid, parts of which may have precipitation and other parts of which are not experiencing rain. Hence, the TG has the lower CSI at 5- to 30-min scales when compared with the PR, TMI, or COM. When the time scale increases from 5 min to 30 days, the CSI for the TG steadily increases from 0.29 to 0.98 as the sampling problem diminishes. The CSI for TG becomes the best among all products when the time scale reaches beyond 3 h because of its best sampling resolution relative to the PR and TMI. The CSI for the PR, TMI, or COM drastically decreases to the lowest values at the time scale of 1 day and then quickly increases as the time scale further increases. This can be explained similarly to the way it is in the above correlation analysis.

4. Summary and conclusions

In this study, 12 years of GV rain products (GR and TG) from the TRMM GV site at MELB are utilized to evaluate TRMM satellite rain products (PR, TMI, and COM). The GR and TG rain rates are matched to the PR, TMI, and COM rain estimates at a grid resolution of 0.25° and various time scales. The error characteristics and rain detection skills of these products are evaluated through intercomparisons with each other. Analyses of mean yearly rain rates and monthly average rain rate show little difference between the two GV products since the GR 2A53 uses TG 2A56 as a constraint on a monthly basis, a result consistent with the design of the 2A53 algorithm. Large disagreements exist between the TG and GR at shorter time scales, however, because of their different spatial and temporal sampling characteristics. The agreement between the TG and GR, measured by the correlation, relative error, and CSI, steadily improves as the time scale increases from 5 min to 30 days. This result is different when comparing the GR with three satellite

products. The agreements decrease to minimum at the time scale of 1–2 days and then increase with increasing time scale as sample errors diminish.

The yearly biases for the PR and TMI relative to the GR are mainly negative, with a few exceptions. The COM bias fluctuates from year to year over the period. In the lower range of rain rates, the PR, TMI, and COM are in good overall agreement with the GR, but the agreement becomes poorer at higher rain rates. The TRMM PR, TMI, and COM fairly well reproduce the diurnal cycle of rainfall observed by the GR and TG, but there is about a 1-h time lag for the satellite relative to the GV, which has been documented in previous studies (e.g., Negri et al. 2002).

It is important to note that the evaluation of TRMM rain estimates in this study is carried out over the land area of central Florida. The results drawn from this limited land area might not be applicable to oceanic areas and other land sites because the rainfall error statistics can be highly regime dependent (e.g., Nesbitt et al. 2004; Berg et al. 2006). In addition, the GV estimates themselves contain some biases, although they are often used as a reference in the TRMM satellite validation. Nevertheless, the GV measurements provide an independent ground-based reference for comparison with TRMM satellite rain estimates, which can aid in the improvement of space-based rain retrieval algorithms for the TRMM and anticipated Global Precipitation Measurement (GPM) satellites.

Acknowledgments. This study was funded under NASA Grant NNG06HX18C. The authors thank Dr. Ramesh Kakar (NASA Headquarters), Dr. Scott Braun (TRMM Project Scientist), and Dr. Arthur Hou (GPM Project Scientist) for their support of this effort. We also greatly appreciate the efforts of Dr. Erich Stocker of the TRMM Science and Data Information System (TSDIS) and NASA Precipitation Processing System (PPS) for generating the 0.25° TRMM data used in this study. We also thank TRMM GV colleagues D. A. Marks and J. L. Pippitt for providing TRMM Standard Product 2A53 and KMLB radar gap information. Thanks also are given to support staff at Kennedy Space Center, the South Florida Water Management District, and St. John's River Water Management District for their routine operation of the rain gauge networks. Special thanks are given to two anonymous reviewers for their insightful comments and stimulating questions.

REFERENCES

Adler, R. F., and Coauthors, 2003: The version 2 Global Precipitation Climatology Project (GPCP) monthly precipitation analysis (1979–present). *J. Hydrometeor.,* **4,** 1147–1167.

Amitai, E., 2000: Systematic variation of observed radar reflectivity–rainfall rate relations in the tropics. *J. Appl. Meteor.,* **39,** 2198–2208.

——, L. Liao, X. Llort, and R. Meneghini, 2005: Accuracy verification of spaceborne radar estimates of rain rate. *Atmos. Sci. Lett.,* **6,** 2–6.

Anagnostou, E. N., C. A. Morales, and T. Dinku, 2001: The use of TRMM precipitation radar observations in determining ground radar calibration biases. *J. Atmos. Oceanic Technol.,* **18,** 616–628.

Berg, W., T. L'Ecuyer, and C. Kummerow, 2006: Rainfall climate regimes: The relationship of regional TRMM rainfall biases to the environment. *J. Appl. Meteor. Climatol.,* **45,** 434–454.

Betts, A. K., and C. Jakob, 2002: Evaluation of the diurnal cycle of precipitation, surface thermodynamics, and surface fluxes in the ECMWF model using LBA data. *J. Geophys. Res.,* **107,** 8045, doi:10.1029/2001JD000427.

Bowman, K. P., 2005: Comparison of TRMM precipitation retrievals with rain gauge data from ocean buoys. *J. Climate,* **18,** 178–190.

Ciach, J. G., and W. F. Krajewski, 1999: On the estimation of radar rainfall error variance. *Adv. Water Resour.,* **22,** 585–595.

Dinku, T., F. Ruiz, S. J. Connor, and P. Ceccato, 2010: Validation and intercomparison of satellite rainfall estimates over Colombia. *J. Appl. Meteor. Climatol.,* **49,** 1004–1014.

Ebert, E. E., J. E. Janowiak, and C. Kidd, 2007: Comparison of near-real-time precipitation estimates from satellite observations and numerical models. *Bull. Amer. Meteor. Soc.,* **88,** 47–64.

Fisher, B. L., 2004: Climatological validation of TRMM TMI and PR monthly rain products over Oklahoma. *J. Appl. Meteor.,* **43,** 519–535.

——, 2007: Statistical error decomposition of regional-scale climatological precipitation estimates from the Tropical Rainfall Measuring Mission (TRMM). *J. Appl. Meteor. Climatol.,* **46,** 791–813.

Gabella, M., J. Joss, G. Perona, and S. Michaelides, 2006: Range adjustment for ground-based radar, derived with the spaceborne TRMM precipitation radar. *IEEE Trans. Geosci. Remote Sens.,* **44,** 126–133.

Haddad, Z. S., E. A. Smith, C. D. Kummerow, T. Iguchi, M. R. Farrar, S. L. Durden, M. Alves, and W. S. Olson, 1997: The TRMM 'day-1' radar/radiometer combined rain-profiling algorithm. *J. Meteor. Soc. Japan,* **75,** 799–809.

Hitschfeld, W., and J. Bordan, 1954: Errors inherent in the radar measurements of rainfall at attenuating wavelengths. *J. Meteor.,* **11,** 58–67.

Hsu, K. L., H. V. Gupta, X. Gao, and S. Sorooshian, 1999: Estimation of physical variables from multi-channel remotely sensed imagery using a neural network: Application to rainfall estimation. *Water Resour. Res.,* **35,** 1605–1618.

Huffman, G. J., and Coauthors, 1997: The Global Precipitation Climatology Project (GPCP) combined precipitation datasets. *Bull. Amer. Meteor. Soc.,* **78,** 5–20.

——, and Coauthors, 2007: The TRMM Multisatellite Precipitation Analysis (TMPA): Quasi-global, multiyear combined-sensor precipitation estimates at fine scales. *J. Hydrometeor.,* **8,** 38–55.

Iguchi, T., and R. Meneghini, 1994: Intercomparison of single-frequency methods for retrieving a vertical rain profile from airborne or spaceborne radar data. *J. Atmos. Oceanic Technol.,* **11,** 1507–1516.

——, T. Kozu, R. Meneghini, J. Awaka, and K. Okamoto, 2000: Rain-profiling algorithm for the TRMM precipitation radar. *J. Appl. Meteor.,* **39,** 2038–2052.

Joyce, R. J., J. E. Janowiak, P. A. Arkin, and P. Xie, 2004: CMORPH: A method that produces global precipitation estimates from passive microwave and infrared data at high spatial and temporal resolution. *J. Hydrometeor.,* **5,** 487–503.

Kummerow, C., W. S. Olson, and L. Giglio, 1996: A simplified scheme for obtaining precipitation and vertical hydrometeor profiles from passive microwave sensors. *IEEE Trans. Geosci. Remote Sens.,* **34,** 1213–1232.

——, and Coauthors, 2001: The evolution of the Goddard profiling algorithm (GPROF) for rainfall estimation from passive microwave sensors. *J. Appl. Meteor.,* **40,** 1801–1840.

Negri, A. J., L. Xu, and R. F. Adler, 2002: A TRMM-calibrated infrared rainfall algorithm applied over Brazil. *J. Geophys. Res.,* **107,** 8048, doi:10.1029/2000JD000265.

Nesbitt, S. W., and E. J. Zipser, 2003: The diurnal cycle of rainfall and convective intensity according to three years of TRMM measurements. *J. Climate,* **16,** 1456–1475.

——, ——, and C. Kummerow, 2004: An examination of version-5 rainfall estimates from the TRMM Microwave Imager, precipitation radar, and rain gauges on global, regional, and storm scales. *J. Appl. Meteor.,* **43,** 1016–1036.

Okamoto, K., T. Iguchi, N. Takahashi, T. Ushio, J. Awaka, S. Shige, and T. Kubota, 2007: High precision and high resolution global precipitation map from satellite data. *Proc. ISAP,* Kaohsiung, Taiwan, Intelligent System Applications to Power Systems, 506–509.

Olson, W. S., and Coauthors, 2006: Precipitation and latent heating distributions from satellite passive microwave radiometry. Part I: Improved method and uncertainty estimates. *J. Appl. Meteor. Climatol.,* **45,** 702–720.

Rosenfeld, D., D. B. Wolff, and E. Amitai, 1994: The window probability matching method for rainfall measurements with radar. *J. Appl. Meteor.,* **33,** 682–693.

Serra, Y. L., and M. J. McPhaden, 2003: Multiple time- and space-scale comparisons of ATLAS buoy rain gauge measurements with TRMM satellite precipitation measurements. *J. Appl. Meteor.,* **42,** 1045–1059.

Sieck, L. C., S. J. Burges, and M. Steiner, 2007: Challenges in obtaining reliable measurements of point rainfall. *Water Resour. Res.,* **43,** W01420, doi:10.1029/2005WR004519.

Smith, E. A., F. J. Turk, M. R. Farrar, A. Mugnai, and X. Xiang, 1997: Estimating 13.8-GHz path-integrated attenuation from 10.7-GHz brightness temperatures for TRMM combined PR–TMI precipitation algorithm. *J. Appl. Meteor.,* **36,** 365–388.

Sohn, B. J., H.-J. Han, and E.-K. Seo, 2010: Validation of satellite-based high-resolution rainfall products over the Korean Peninsula using data from a dense rain gauge network. *J. Appl. Meteor. Climatol.,* **49,** 701–714.

Sorooshian, S., K. Hsu, X. Gao, H. V. Gupta, B. Imam, and D. Braithwaite, 2000: Evaluation of PERSIANN system satellite-based estimates of tropical rainfall. *Bull. Amer. Meteor. Soc.,* **81,** 2035–2046.

Stocker, E. F., J. Kwiatkowski, and O. Kelley, 2001: Gridded hourly text products: A TRMM data reduction approach. *Proc. 2001 Int. Geoscience and Remote Sensing Symp.,* Sydney, NSW, Australia, IEEE, 658–660.

Tian, Y., C. D. Peters-Lidard, B. J. Choudhury, and M. Garcia, 2007: Multitemporal analysis of TRMM-based satellite precipitation products for land data assimilation applications. *J. Hydrometeor.,* **8,** 1165–1183.

Turk, F. J., and S. D. Miller, 2005: Toward improving estimates of remotely sensed precipitation with MODIS/AMSR-E blended data techniques. *IEEE Trans. Geosci. Remote Sens.,* **43,** 1059–1069.

Vasiloff, S., and Coauthors, 2007: Improving QPE and very short term QPF: An initiative for a community-wide integrated approach. *Bull. Amer. Meteor. Soc.,* **88,** 1899–1911.

Wang, J., and D. B. Wolff, 2009: Comparisons of reflectivities from the TRMM precipitation radar and ground-based radars. *J. Atmos. Oceanic Technol.,* **26,** 857–875.

——, and ——, 2010: Evaluation of TRMM ground-validation radar-rain errors using rain gauge measurements. *J. Appl. Meteor. Climatol.,* **49,** 310–324.

——, B. L. Fisher, and D. B. Wolff, 2008: Estimating rain rates from tipping-bucket rain gauge measurements. *J. Atmos. Oceanic Technol.,* **25,** 43–56.

Wilks, D. S., 1995: *Statistical Methods in the Atmospheric Sciences: An Introduction*. Academic Press, 467 pp.

Wolff, D. B., and B. L. Fisher, 2008: Comparisons of instantaneous TRMM ground validation and satellite rain-rate estimates at different spatial scales. *J. Appl. Meteor. Climatol.,* **47,** 2215–2237.

——, D. A. Marks, E. Amitai, D. S. Silberstein, B. L. Fisher, A. Tokay, J. Wang, and J. L. Pippitt, 2005: Ground validation for the Tropical Rainfall Measuring Mission (TRMM). *J. Atmos. Oceanic Technol.,* **22,** 365–380.

Xie, P., and P. A. Arkin, 1997: Global precipitation: A 17-year monthly analysis based on gauge observations, satellite estimates, and numerical model outputs. *Bull. Amer. Meteor. Soc.,* **78,** 2539–2558.

Yang, S., and E. A. Smith, 2006: Mechanisms for diurnal variability of global tropical rainfall observed from TRMM. *J. Climate,* **19,** 5190–5226.